JOURNAL OF VIROLOGY, Nov. 2010, p. 11145–11151 Vol. 84, No. 21
0022-538X/10/$12.00 doi:10.1128/JVI.00036-10

Structural Evidence of Glycoprotein Assembly in Cellular Membrane Compartments prior to Alphavirus Budding▽†

Pan Soonsawad,[1,4,5] Li Xing,[1] Emerson Milla,[1] Juan M. Espinoza,[1] Masaaki Kawano,[1] Michael Marko,[2] Chyongere Hsieh,[2] Hiromitsu Furukawa,[3] Masahiro Kawasaki,[3] Wattana Weerachatyanukul,[4] Ranjana Srivastava,[6] Susan W. Barnett,[6] Indresh K. Srivastava,[6] and R. Holland Cheng[1]*

Department of Molecular and Cellular Biology, University of California, Davis, California 95616-8536[1]; Resources for Visualization of Biological Complexity, Wadsworth Center, Albany, New York 12201[2]; Japan Electron Optics Laboratory System and Technology Co., 3-1-2 Musashino, Tokyo, Japan[3]; Department of Anatomy, Faculty of Science, Mahidol University, Bangkok, Thailand[4]; Faculty of Dentistry, Mahidol University, Bangkok, Thailand[5]; and Novartis Vaccines and Diagnostics, Inc., 350 Massachusetts Ave., Cambridge, Massachusetts 02139[6]

Received 8 January 2010/Accepted 17 August 2010

Membrane glycoproteins of alphavirus play a critical role in the assembly and budding of progeny virions. However, knowledge regarding transport of viral glycoproteins to the plasma membrane is obscure. In this study, we investigated the role of cytopathic vacuole type II (CPV-II) through *in situ* electron tomography of alphavirus-infected cells. The results revealed that CPV-II contains viral glycoproteins arranged in helical tubular arrays resembling the basic organization of glycoprotein trimers on the envelope of the mature virions. The location of CPV-II adjacent to the site of viral budding suggests a model for the transport of structural components to the site of budding. Thus, the structural characteristics of CPV-II can be used in evaluating the design of a packaging cell line for replicon production.

Semliki Forest virus (SFV) is an enveloped alphavirus belonging to the family *Togaviridae*. This T=4 icosahedral virus particle is approximately 70 nm in diameter (30) and consists of 240 copies of E1/E2 glycoprotein dimers (3, 8, 24). The glycoproteins are anchored in a host-derived lipid envelope that encloses a nucleocapsid, made of a matching number of capsid proteins and a positive single-stranded RNA molecule. After entry of the virus via receptor-mediated endocytosis, a low-pH-induced fusion of the viral envelope with the endosomal membrane delivers the nucleocapsid into the cytoplasm, where the replication events of SFV occur (8, 19, 30). Replication of the viral genome and subsequent translation into structural and nonstructural proteins followed by assembly of the structural proteins and genome (7) lead to budding of progeny virions at the plasma membrane (18, 20). The synthesis of viral proteins shuts off host cell macromolecule synthesis, which allows for efficient intracellular replication of progeny virus (7). The expression of viral proteins leads to the formation of cytopathic vacuolar compartments as the result of the reorganization of cellular membrane in the cytoplasm of an infected cell (1, 7, 14).

Early studies using electron microscopy (EM) have characterized the cytopathic vacuoles (CPVs) in SFV-infected cells (6, 13, 14) and identified two types of CPV, namely, CPV type I (CPV-I) and CPV-II. It was found that CPV-I is derived from modified endosomes and lysosomes (18), while CPV-II is derived from the *trans*-Golgi network (TGN) (10, 11). Significantly, the TGN and CPV-II vesicles are the major membrane compartments marked with E1/E2 glycoproteins (9, 11, 12). Inhibition by monensin results in the accumulation of E1/E2 glycoproteins in the TGN (12, 26), thereby indicating the origin of CPV-II. While CPV-II is identified as the predominant vacuolar structure at the late stage of SFV infection, the exact function of this particular cytopathic vacuole is less well characterized than that of CPV-I (2, 18), although previous observations have pointed to the involvement of CPV-II in budding, because an associated loss of viral budding was observed when CPV-II was absent (9, 36).

In this study, we characterized the structure and composition of CPV-II in SFV-infected cells *in situ* with the aid of electron tomography and immuno-electron microscopy after physical fixation of SFV-infected cells by high-pressure freezing and freeze substitution (21, 22, 33). The results revealed a helical array of E1/E2 glycoproteins within CPV-II and indicate that CPV-II plays an important role in intracellular transport of glycoproteins prior to SFV budding.

MATERIALS AND METHODS

Cell culture and virus infection. Baby hamster kidney-21 (BHK-21) cells were maintained in minimum essential medium (MEM; Gibco) supplemented with 10% fetal bovine serum (Sigma), 100 IU/ml penicillin-streptomycin, and 50 ml tryptose phosphate broth in an atmosphere of 5% CO_2. Subconfluent monolayers of BHK-21 cells were first washed twice with phosphate-buffered saline (PBS; Gibco) and then mixed with SFV at a multiplicity of infection (MOI) of 200. After 30 min of adsorption, the virus-containing medium was replaced with fresh minimum essential medium (MEM) after washing with PBS twice and the cells were further incubated at 37°C for 3, 5, or 8 h postinfection (hpi) (5, 15).

Preimmunolabeling. The SFV-infected cells were incubated with anti-E2 monoclonal antibody (1:100 dilution) for 45 min on ice and washed 3 times with PBS-bovine serum albumin (BSA) (29). This was followed by the addition of protein A-conjugated 10-nm gold (1:300 dilution), followed by the washing steps

* Corresponding author. Mailing address: Department of Molecular and Cellular Biology, University of California, Davis, CA 95616-8536. Phone: (530) 752-5659. Fax: (530) 752-3085. E-mail: rhch@ucdavis.edu.

† Supplemental material for this article may be found at http://jvi.asm.org/.

▽ Published ahead of print on 8 January 2010.

described above. Subsequently, the cells were transferred on ice before high-pressure freezing.

High-pressure freezing and freeze substitution. Infected BHK-21 cells were loaded into flat specimen holders and mounted on a PACT HPF station (Leica Microsystems, Vienna, Austria), directly frozen, and transferred into liquid nitrogen (34). The samples were freeze substituted in 0.2% glutaraldehyde and 0.1% uranyl acetate in acetone at −90°C for 72 h and then warmed up slowly to −20°C (automatic freeze substitution [AFS] system; Leica Microsystems). After being rinsed several times in acetone, the cells were infiltrated in a resin-ethanol mixture with a gradually increasing ratio of Lowicryl to ethanol (1:3, 1:1, and 3:1) and in pure Lowicryl for the final infiltration. The resin polymerization was performed at 50°C with UV light. The sample blocks were thin sectioned with a Leica microtome, and serial sections (80 nm to 150 nm thick) were collected on Formvar-coated, carbon-stabilized, one-slot copper grids.

Postimmunolabeling. Sections of embedded sample were first treated with 0.1 M ammonium chloride for 10 min followed by blocking with 1% PBS-BSA for 15 min. After incubation with primary antibodies (at a 1:50 dilution for both anti-E1 and anti-E2 antibodies) overnight at 4°C, the section was washed with PBS and then incubated for 1 h with protein A-conjugated 10-nm gold (1:300 dilution) followed by another wash with PBS. For better binding of gold to the target antigen, the labeled section was further fixed with 1% glutaraldehyde for 10 min and then washed with deionized water.

Electron tomography. The EM sections were first screened using a JEOL 1230 electron microscope operated at 120 kV. The electron dose for each image was 500 to 1,000 e^-/nm^2, and the micrographs were recorded with a charge-coupled-device (CCD) camera (TVIPS Gauting) with a pixel resolution of 2,000 by 2,000. The magnification of the microscope was calibrated by using tobacco mosaic virus as a standard, and the CPV-II size was normalized accordingly. After image screening, tomographic data acquisition was done using a JEOL 2100F EM with a field emission gun (FEG) operated at 200 kV. The recording and reconstruction scaling factor was 1.0 nm/pixel, and the electron dose per image was 500 e^-/nm^2 (3, 22, 34). Tomograms were collected at one-degree tilt intervals between −60° and +60° at ×15,000 magnification with a CCD camera (TVIPS Gauting) with a pixel resolution of 4,000 by 4,000, using automated recording software (JEOL System Technology Co., Ltd.) that utilized cross-correlation to center the images. The collected images in the tilt series were aligned by using 10-nm gold particles as markers to eliminate image displacement and to refine the relative tilt angle. After alignment, the image reconstruction was performed and the tomogram was computed to a resolution of 4 nm by weighted back projection (17, 23, 34). The obtained tomogram was then analyzed with visualization programs. Volume rendering of density maps were done with UCSF Chimera (http://www.cgl.ucsf.edu/chimera) and Amira (Visage Imaging, San Diego, CA) (35). Movies were prepared with both the JEOL visualization program (JEOL System Technology Co., Ltd.) and UCSF Chimera.

RESULTS

Presence of CPV-II near the cell surface at late stages of infection. To better understand the function of CPV-II, we investigated the distribution of CPV-II in relation to the intensity of SFV replication. There appeared to be no uniform shape of CPV-II in the cytosol of SFV-infected baby hamster kidney-21 (BHK-21) cells. CPV-II was found throughout the cytosol and interspersed among other empty vacuoles (see Fig S1 in the supplemental material), particularly near the cell surface (Fig. 1A). A higher multiplicity of infection (MOI) did not induce an earlier appearance of CPV-II: no CPV-II was found in the cells at 3 h postinfection (hpi) regardless of what MOI we used (Fig. 1B). At 5 hpi, the cells that were infected at an MOI of 200 revealed clusters of CPV-II at the perinuclear region (Fig. S1A). At this time point, the CPV-II number in the cells infected at an MOI of 200 was found to be 3-fold higher than that in the cells infected with an MOI of 2 (*P* value, 0.0022) (Fig. 1B). At 8 hpi, CPV-II was found throughout the cytoplasm, and some of the CPV-II was located close to the plasma membrane (Fig. 1A; see Fig. S1B in the supplemental material). At this time point, the CPV-II numbers of the cells infected with an MOI of 200 and the cells infected with an MOI of 2 did not appear to be significantly different (*P* value, 0.355). When the virus adsorption at an MOI of 2 was increased from 0.5 h to 1 h, the number of type II CPVs at 5 hpi gradually increased above that corresponding to an MOI of 2 for 0.5 h but was still significantly different from that corresponding to an MOI of 200 for 0.5 h (*P* value, 0.077). However, at 8 hpi, the number of type II CPVs appeared no different from that corresponding to an MOI of 200 (*P* value, 0.996) (Fig. 1B). Therefore, intensive viral infection results in rapid increase of CPV-II numbers in the cytoplasm.

Morphological features of CPV-II. To get insights into CPV-II morphology, we traced a type II CPV in a series of consecutive sections. CPV-II was first observed as a cluster of electron-dense particles (~30 nm in diameter), then as a vacuole containing multiple tubular structures in the next few slices, and then again as a cluster of electron-dense particles (Fig. 1C). Therefore, CPV-II is a spindle-like compartment that encloses tubular structures and is decorated with electron-dense particles on the exterior surface. While the diameter of CPV-II was observed to be on average 100 to 400 nm (Fig. 1C and D), the longitudinal dimension occasionally exceeded 1 μm (Fig. 1E). The internal tubules were roughly 50 nm in diameter (Fig. 1D to F) and had no particular orientations relative to the boundary membrane of CPV-II (Fig. 1C), although some tubules were observed to vertically contact the membrane of CPV-II (Fig. 2).

Protein arrangement of the tubular structure inside CPV-II. The tubular structure is one of the characteristic features of CPV-II, and its composition was investigated by using immunogold labeling with either anti-E1 or anti-E2 monoclonal antibodies. By using anti-E2 antibody, we found that the gold particles were selectively attached to the tubular structures within CPV-II (Fig. 2A), indicating that the tubules contained E2 glycoproteins. The same result was observed when anti-E1 antibodies were used (see Fig. S2 in the supplemental material). This observation agrees well with the findings that the E1/E2 heterodimer formed in the endoplasmic reticulum (ER) and transported as a dimer via the cell secretory pathway (26). We then investigated the three-dimensional (3D) structure of CPV-II with electron tomography. A tilt series was collected with this type II CPV, which was immunogold labeled with anti-E2 antibody, and a 3D tomogram was computed after the images were aligned into a common coordinate system by using the gold particles as fiducial register for image alignment. The tomogram revealed that the tubular structure is in a quasihelical arrangement, as it was clearly seen during slicing of the tomogram along the *z* axis with an interval of 0.67-nm slices (Fig. 2B; see Video S1 in the supplemental material).

Correlation between tubular structure and the isolated SFV. Detailed tomographic analysis of tubules within CPV-II showed that the density nodes, bright spots in the images representing high electron density, arranged into a hexagonal lattice with one density node per hexagonal vertex (Fig. 2C). The helical lattice on the tubule was found to resemble the surface lattice of the glycoproteins on the envelope of a mature virion (Fig. 2D), as revealed by the reconstruction of mature viruses from cryo-electron microscopy (cryo-EM) (15). The average distance between nodes measured from the hexagonal lattice on the CPV-II tubule was ~7 nm, similar to the distance between glycoprotein trimers on the mature virus (Fig. 2C and D), the

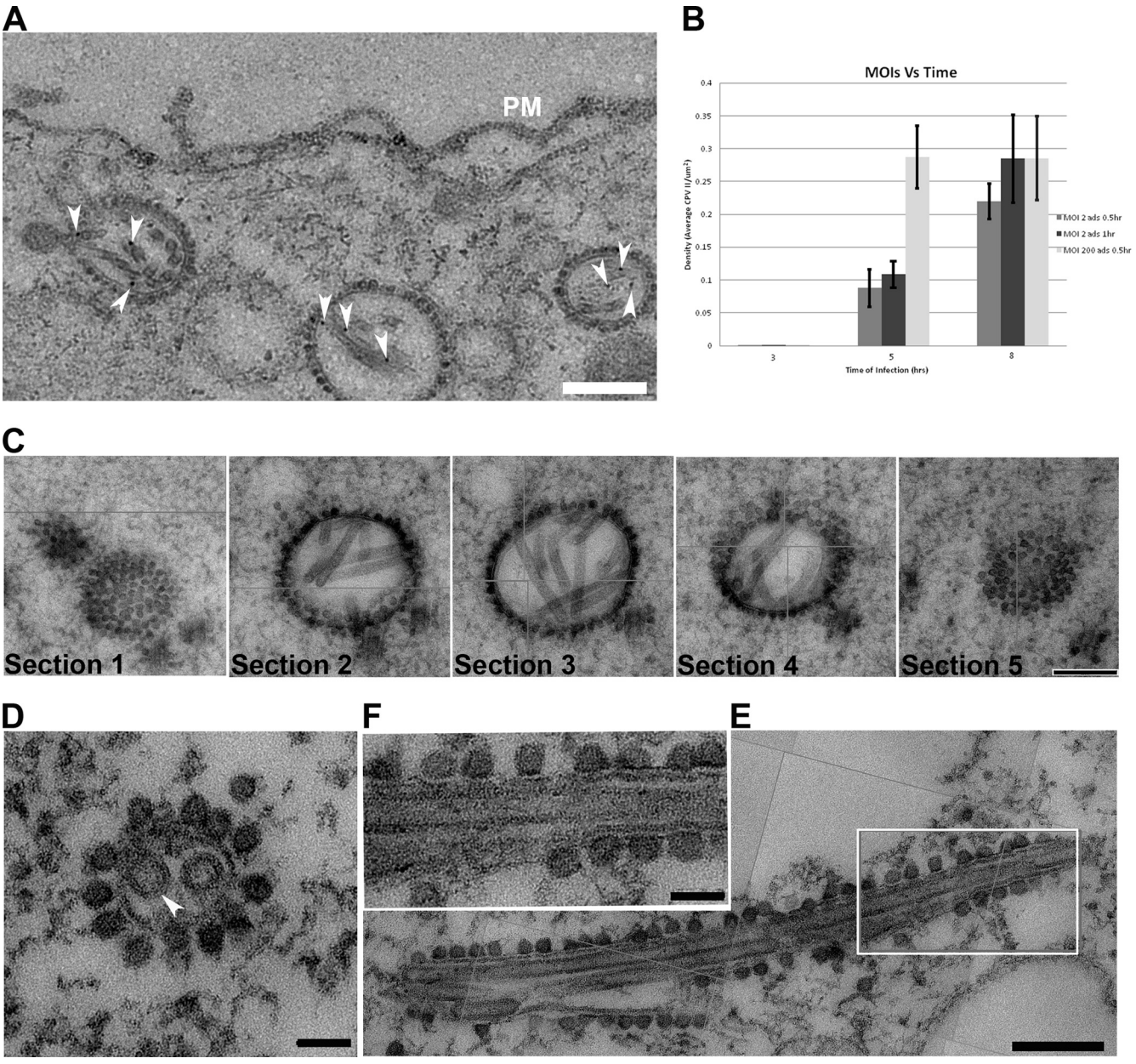

FIG. 1. CPV-II distribution and morphology in SFV-infected BHK-21 cells. (A) CPV-II can be found close to the plasma membrane at the late stage of SFV infection. Tubular structures were well preserved in CPV-II and attached by gold particles (white arrowheads) that registered the location of anti-E2 antibodies. The gold particle was identified by its unique profile, the darkest-contrast and sharply defined edge. A few gold particles located on the plasma membrane are not marked. (B) The plot shows the CPV-II density in the BHK-21 cells that were infected with SFV at an MOI of 2 for 30 min, an MOI of 2 for 60 min, and an MOI of 200 for 30 min. The number of type II CPVs was counted after fixation of the cells at 3, 5, and 8 h postinfection and normalized relative to the measured specimen area. The average CPV-II density (number per μm^2) $\pm$ standard deviation (SD) at each time point is shown. There was no CPV-II observed in mock-infected BHK-21 cells; thus the mock infection data were omitted from the graph. ads, adsorption. (C) Five consecutive sections (95 nm thick) of the same type II CPV, showing the CPV from the top to bottom. (D) A view of a CPV-II enclosed tubular structure (white arrowhead), attached by dense circular particles on the exterior surface. The two tubules within CPV-II are approximately 50 nm in diameter. (E) A longitudinal section of CPV-II shows its dimension (exceeding 1 μm). (F) A zoomed-in image of the area enclosed in a white box in panel E, showing the dense particles attached to the external membrane layer of CPV-II and the tubules. Scale bars, 200 nm (panels A, C, and E) and 50 nm (panels D and F).

glycoprotein network observed just outside the viral membrane. Therefore, the density nodes at the tubular structure may represent the location of the E1/E2 trimers.

The relevance of the cytopathic vacuole in SFV budding at the plasma membrane. At a late stage of virus budding, while the viral envelope is still associated with the plasma membrane, the capsid-membrane interface is semiopen, and the budding particles appeared as an incomplete circular profile (Fig. 3A and B). The SFV-infected cell labeled with anti-E2 antibodies revealed that the conjugated gold markers

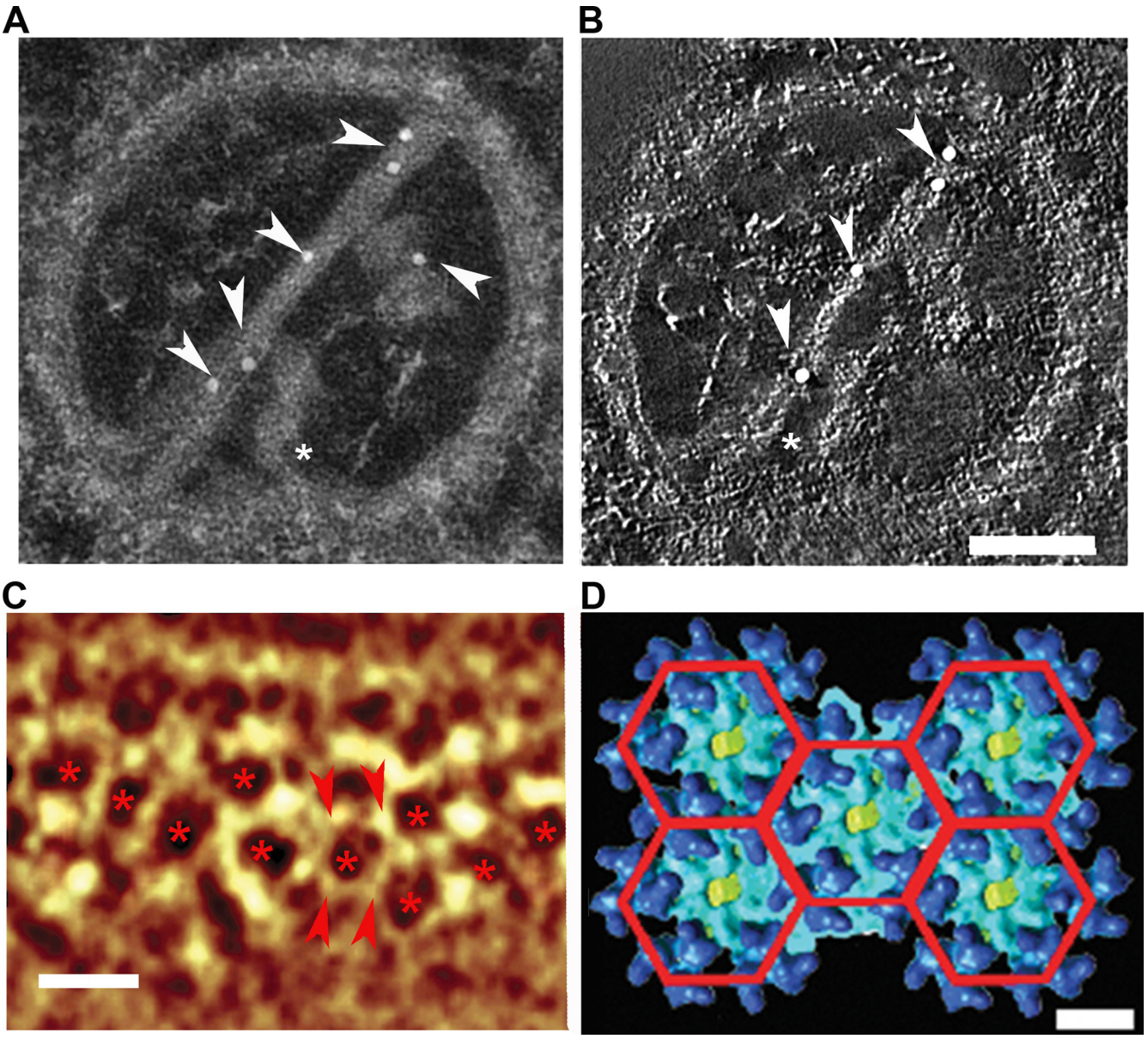

FIG. 2. The composition of a CPV-II tubular structure. (A) The gold particles (arrowheads) were attached to the tubular structures of the tomogram of CPV-II during immunolabeling with anti-E2 antibody. Additional short tubules were observed lying vertically to the long tubules, and one of them (asterisk) appears to make contact with the CPV-II membrane. (B) An orthoslice (0.67 nm in thickness) was taken from the tomogram of the same CPV-II as in panel A, showing two tubules that appeared to have helical turns. The gold particle on the short tube is omitted from the slice, as it was positioned on the other side of the section (see also Video S1 in the supplemental material). Note that the gold labeling was performed on both sides, and it resulted in an uneven distribution of gold particles in the *z* dimension. Scale bar, 100 nm. (C) Volume rendering of CPV-II tubule tomogram shows the hexagonal array (asterisks) of the density nodes. Scale bar, 15 nm. The node-to-node distance (between the pair of arrowheads) is approximately 7 nm. (D) A planar array of five adjacent hexagonal rings of SFV glycoprotein trimers indicates that the trimer-to-trimer distance is 7.2 nm. Scale bar, 7 nm.

were located in the areas proximal to the budding site (Fig. 3; see Video S2 in the supplemental material), indicating that some glycoprotein-capsid interactions occur concurrently on the plasma membrane with virus budding, consistent with previous observations (27, 28, 31). As gold-particle-conjugated anti-E2 antibodies were similarly observed at the surface of budded SFV virions, the viral envelope should indeed be derived from the plasma membrane of the infected cell (Fig. 3B). On the outer leaflet of the plasma membrane around the virus budding region, the majority of gold particles were observed marking the viral glycoproteins, with an average distance of ~7 nm in spacing.

The envelope of budding virions on the plasma membrane. To better understand SFV assembly at the plasma membrane, we characterized the morphology of SFV particles during budding with electron tomography and compared the intertrimer distance on the envelope of nearly mature virions with that of the mature virions. The spike feature on the budding particle

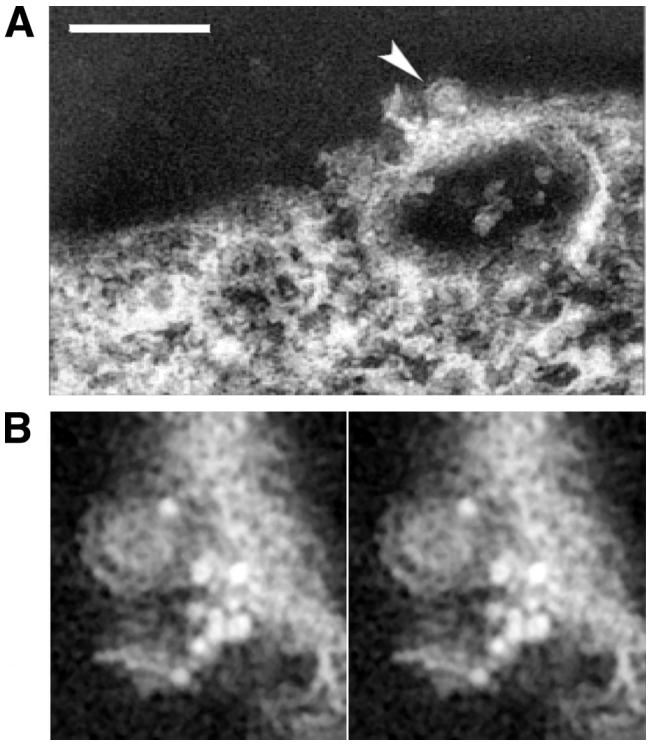

FIG. 3. Arrangement of viral glycoproteins at the site of budding on the plasma membrane. (A) A volume projection of SFV budding site reveals that the budding virus (arrowhead) was in proximity to the gold particles that registered the location of the E2 glycoprotein on the plasma membrane. Scale bar, 200 nm. (B) The stereo pair of projection views above plasma membrane illustrates the budding region around an exiting virion (arrowhead in panel A). This close-up view shows the exterior surface of the plasma membrane with detailed arrangement of an associated group of gold markers, with the majority of them observed with an average spacing of ~7 nm. The conjugated gold particles are located on the plasma membrane with the brightest density as a result of the high-angle electron scattering in electron microscopic imaging.

(Fig. 4C) appeared to have a hexagonal lattice and distance between the spikes similar to those on the mature viral particles (Fig. 4B), although the symmetry of the budding virion from the tomogram is not perfect. This defective symmetry could come from the stage of budding, where the viral particle was partially formed and had not been released from the host cell. The nearly budded virions appeared to have protruding spikes, which were on average 5 to 6 nm in height. Importantly, the distance between adjacent spikes was measured to be 7 to 8 nm (Fig. 4C). These dimensions correspond well with the hexagonal lattices measured from the cryo-EM density map of the mature virions (15, 35).

DISCUSSION

Infection by enveloped viruses, like SFV, induces membrane reorganization within the cell and the appearance of cytopathic vacuoles (CPVs). Here, we reported the structure and composition of CPV-II, a membrane vacuole appearing at later stages of SFV infection, in order to reveal its function in SFV replication. CPV-II appeared as spindle-shaped vacuoles that were not found within 3 hpi and were distributed in correlation with the time of postinfection. Tubular structures are one of the characteristic features within CPV-II and are composed of E1/E2 glycoproteins. The viral glycoproteins arrange themselves in hexagonal arrays (Fig. 2; see Video S1 in the supplemental material), in which the distance between the density nodes matched that between the glycoproteins on the budding viral particles (see Video S2 in the supplemental material), resembling the organization of E1/E2 trimers on the envelope of the mature virion (3, 15). The results described above suggest that the well-organized viral lattices may be initiated from clusters of E1/E2 hexagonal arrays inside the CPV-II compartment and transfer into the adjoining E1/E2 hexameric rings in part of viral envelope upon virus budding (Fig. 5). Any subsequent budding assembly of the virus would benefit from the predominant E1/E2 arrays on the plasma membrane and the E1/E2 hexagonal patches on the tubular structure. Over the course of SFV budding, the hexagonally organized glycoproteins could in turn organize the capsid proteins and the associated viral genome underneath the cell membrane to fulfill a stoichiometric 1:1 ratio of E1/E2 heterodimer to the capsid protein (3). CPV-II thus provides a transport vehicle to send the E1/E2 viral glycoproteins from the TGN to the viral budding sites on the plasma membrane. This theory is further substantiated by the observation of abundant CPV-II at the region close to the plasma membrane at a later time point of virus infection and is in good agreement with a previously report (36). CPV-II could also provide a reservoir of glycoproteins destined for the plasma membrane to eventually assemble into the mature virus by budding.

Here, the icosahedral symmetry on the nucleocapsid may occur concurrently with the budding in the guidance of the glycoprotein lattice (3, 5). The binding of capsid protein to single-stranded RNA occurs quickly after protein synthesis, and the appearance of the 150S nucleoprotein complex was detected from the cytoplasm (4, 32). The dense particles observed on the CPV-II membrane appeared similar in size and appearance to those nucleocapsids in the budding virions (see Fig. S3 in the supplemental material). It is tempting to speculate that CPV-II transports both the viral glycoprotein and the nucleocapsid complex to the plasma membrane. This would increase the concentrations of both capsid protein and glycoproteins at the site of budding and perhaps lead to the subsequent interactions of the capsid protein with the viral glycoproteins to complete the SFV assembly at the plasma membrane (3, 8, 29). Such speculation is supported by the finding on membrane-protein-directed SFV assembly, for which the glycoproteins were observed to direct the assembly of nucleocapsid core, regardless of the deficient formation of preformed nucleoprotein core in the cytoplasm (4, 5). However, more-detailed evidence, which includes direct tracking of viral structural proteins during the process of budding and exploring the transition of the budding capsid from a flexible to a stable particle, is still required. Nevertheless, the hexagonal arrangement of E1/E2 seen in the CPV-II tubules can provide a structural basis to organize the underlying capsid protein into a T=4 nucleocapsid (3, 5) while the plasma membrane is embedded into a curvature wrapping the nucleocapsid.

In conclusion, SFV infection induced the reorganization of the host-cell membrane and the appearance of cytopathic

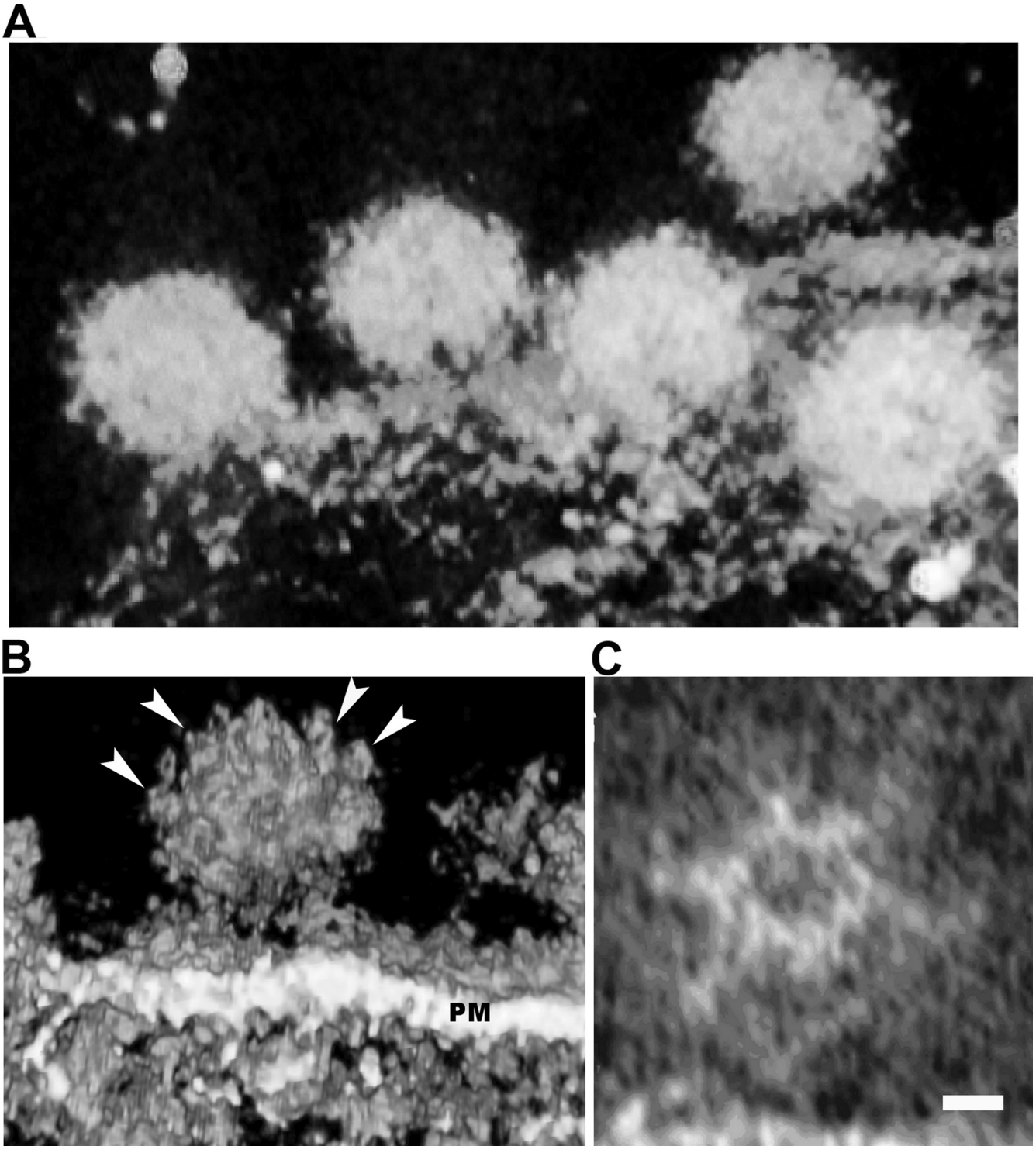

FIG. 4. Array of glycoproteins on budding SFV. (A) A volume rendering of the tomogram on the budding viruses on the plasma membrane of a cell infected with SFV. Several budding virions (~70 nm in diameter) were captured before scission from plasma membrane. (B) Surface rendering of this tomogram showing the interstices of the spikes on the outer envelope of the virion. A budding virion clearly shows the hexagonal array of the glycoproteins (arrowheads), where the node-to-node distance is measured as 7 nm. PM, plasma membrane. (C) A slice section from the tomogram of the same budding virus demonstrates clearly the hexagonal density, corresponding well to the glycoprotein network in the cryo-EM density map of isolated virus. Scale bar, 5 nm.

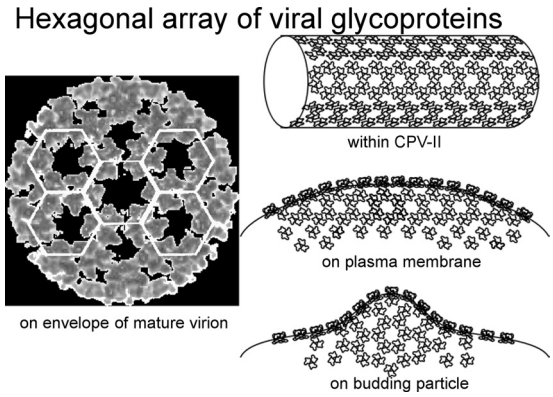

FIG. 5. The SFV glycoproteins arrange into a hexagonal array within CPV-II while in transport to the plasma membrane. A similar array dimension between glycoproteins is observed on the plasma membrane adjacent to the budding virion and subsequently organized into the envelope of a T=4 lattice through the virion assembly to perform membrane budding. These well-defined glycoprotein arrays may help playing important roles in organizing the symmetry of the nucleocapsid in forming a mature virion.

vacuoles (CPV-II) which in turn compartmentalize viral glycoproteins E1 and E2. These glycoproteins are arranged in a tubular structure inside CPV-II during transport to the site of budding on the plasma membrane. To facilitate viral capsid formation through the membrane budding, E1/E2 is likely introduced on the cell surface as a form resembling the pattern of the viral surface lattice at the side of budding. This understanding of the role of CPV-II in SFV particle replication will further facilitate the development of a criterion to engineer productive cell lines packaging heterologous genes with alphavirus replicon systems (16, 25).

ACKNOWLEDGMENTS

We thank Leevi Kääriäinen, Giuseppe Balistreri, and Selina Poon for their insightful discussions during preparation of the manuscript. Mouse monoclonal antibodies were kindly provided by Margaret Kielian. We thank Joseph Wang and Dominik Green for their assistance with figure production and software management.

This work was sponsored by NIH HIVRAD and Discovery grants.

REFERENCES

1. **Acheson, N. H., and I. Tamm.** 1967. Replication of Semliki Forest virus: an electron microscopic study. Virology **32:**128–143.
2. **Barton, D. J., S. G. Sawicki, and D. L. Sawicki.** 1991. Solubilization and immunoprecipitation of alphavirus replication complexes. J. Virol. **65:**1496–1506.
3. **Cheng, R. H., R. J. Kuhn, N. H. Olson, M. G. Rossmann, H. K. Choi, T. J. Smith, and T. S. Baker.** 1995. Nucleocapsid and glycoprotein organization in an enveloped virus. Cell **80:**621–630.
4. **Forsell, K., G. Griffiths, and H. Garoff.** 1996. Preformed cytoplasmic nucleocapsids are not necessary for alphavirus budding. EMBO J. **15:**6495–6505.
5. **Forsell, K., L. Xing, T. Kozlovska, R. H. Cheng, and H. Garoff.** 2000. Membrane proteins organize a symmetrical virus. EMBO J. **19:**5081–5091.
6. **Friedman, P. N., J. G. Levin, P. M. Grimley, and I. K. Brezesky.** 1972. Membrane-associated replication complex in arbovirus infection. J. Virol. **10:**504–515.
7. **Froshauer, S., J. Kartenbeck, and A. Helenius.** 1988. Alphavirus RNA replicase is located on the cytoplasmic surface of endosomes and lysosomes. J. Cell Biol. **107:**2075–2086.
8. **Garoff, H., and R. H. Cheng.** 2001. The missing link between envelope formation and fusion in alphaviruses. Trends Microbiol. **9:**408–410.
9. **Garoff, H., J. Wilschut, P. Liljestrom, J. M. Wahlberg, R. Bron, M. Suomalainen, J. Smyth, A. Salminen, B. U. Barth, H. Zhao, et al.** 1994. Assembly and entry mechanisms of Semliki Forest virus. Arch. Virol. Suppl. **9:**329–338.
10. **Griffiths, G., S. D. Fuller, R. Back, M. Hollinshead, S. Pfeiffer, and K. Simons.** 1989. The dynamic nature of the Golgi complex. J. Cell Biol. **108:** 277–297.
11. **Griffiths, G., P. Quinn, and G. Warren.** 1983. Dissection of the Golgi complex. I. Monensin inhibits the transport of viral membrane proteins from medial to trans Golgi cisternae in baby hamster kidney cells infected with Semliki Forest virus. J. Cell Biol. **96:**835–850.
12. **Griffiths, G., K. Simons, G. Warren, and K. T. Tokuyasu.** 1983. Immunoelectron microscopy using thin, frozen sections: application to studies of the intracellular transport of Semliki Forest virus spike glycoproteins. Methods Enzymol. **96:**466–485.
13. **Grimley, P. M., I. K. Berezesky, and P. N. Friedman.** 1968. Cytoplasmic structures associated with an arbovirus infection: loci of viral ribonucleic acid synthesis. J. Virol. **2:**1326–1338.
14. **Grimley, P. M., J. G. Levin, I. K. Berezesky, and R. M. Friedman.** 1972. Specific membranous structures associated with the replication of group A arboviruses. J. Virol. **10:**492–503.
15. **Haag, L., H. Garoff, L. Xing, L. Hammar, S. T. Kan, and R. H. Cheng.** 2002. Acid-induced movements in the glycoprotein shell of an alphavirus turn the spikes into membrane fusion mode. EMBO J. **21:**4402–4410.
16. **Karlsson, G. B., and P. Liljestrom.** 2004. Delivery and expression of heterologous genes in mammalian cells using self-replicating alphavirus vectors. Methods Mol. Biol. **246:**543–557.
17. **Kawano, M. A., L. Xing, H. Tsukamota, T. Inoue, H. Handa, and R. H. Cheng.** 2009. Calcium-bridge triggers capsid disassembly in the cell entry process of simian virus 40. J. Biol. Chem. **284:**34703–34712.
18. **Kujala, P., A. Ikaheimonen, N. Ehsani, H. Vihinen, P. Auvinen, and L. Kaariainen.** 2001. Biogenesis of the Semliki Forest virus RNA replication complex. J. Virol. **75:**3873–3884.
19. **Lu, Y. E., T. Cassese, and M. Kielian.** 1999. The cholesterol requirement for Sindbis virus entry and exit and characterization of a spike protein region involved in cholesterol dependence. J. Virol. **73:**4272–4278.
20. **Lu, Y. E., and M. Kielian.** 2000. Semliki Forest virus budding: assay, mechanisms, and cholesterol requirement. J. Virol. **74:**7708–7719.
21. **McEwen, B. F., and M. Marko.** 2001. The emergence of electron tomography as an important tool for investigating cellular ultrastructure. J. Histochem. Cytochem. **49:**553–564.
22. **Noda, T., H. Sagara, A. Yen, A. Takada, H. Kida, R. H. Cheng, and Y. Kawaoka.** 2006. Architecture of ribonucleoprotein complexes in influenza A virus particles. Nature **439:**490–492.
23. **Orlov, I., D. G. Morgan, and R. H. Cheng.** 2006. Efficient implementation of a filtered back-projection algorithm using a voxel-by-voxel approach. J. Struct. Biol. **154:**287–296.
24. **Pletnev, S. V., W. Zhang, S. Mukhopadhyay, B. R. Fisher, R. Hernandez, D. T. Brown, T. S. Baker, M. G. Rossmann, and R. J. Kuhn.** 2001. Locations of carbohydrate sites on alphavirus glycoproteins show that E1 forms an icosahedral scaffold. Cell **105:**127–136.
25. **Polo, J. M., B. A. Belli, D. A. Driver, I. Frolov, S. Sherrill, M. J. Hariharan, K. Townsend, S. Perri, S. J. Mento, D. J. Jolly, S. M. Chang, M. J. Schlesinger, and T. W. Dubensky, Jr.** 1999. Stable alphavirus packaging cell lines for sindbis virus and semliki forest virus-derived vectors. Proc. Natl. Acad. Sci. U. S. A. **96:**4598–4603.
26. **Sariola, M., J. Saraste, and E. Kuismanen.** 1995. Communication of post-Golgi elements with early endocytic pathway: regulation of endoproteolytic cleavage of Semliki Forest virus p62 precursor. J. Cell Sci. **108**(Part 6)**:**2465–2475.
27. **Simons, K., and H. Garoff.** 1980. The budding mechanism of enveloped animal viruses. J. Gen. Virol. **50:**1–21.
28. **Skoging, U., M. Vihinen, L. Nilsson, and P. Liljestrom.** 1996. Aromatic interactions define the binding of the alphavirus spike to its nucleocapsid. Structure **4:**519–529.
29. **Sojakka, K., E. L. Punnonen, and V. S. Marjomaki.** 1999. Isoproterenol inhibits fluid-phase endocytosis from early to late endosomes. Eur. J. Cell Biol. **78:**161–169.
30. **Strauss, J. H., and E. G. Strauss.** 1994. The alphaviruses: gene expression, replication, and evolution. Microbiol. Rev. **58:**491–562.
31. **Suomalainen, M., P. Liljestrom, and H. Garoff.** 1992. Spike protein-nucleocapsid interactions drive the budding of alphaviruses. J. Virol. **66:**4737–4747.
32. **Tellinghuisen, T. L., and R. J. Kuhn.** 2000. Nucleic acid-dependent crosslinking of the nucleocapsid protein of Sindbis virus. J. Virol. **74:**4302–4309.
33. **Wagenknecht, T., C. E. Hsieh, B. K. Rath, S. Fleischer, and M. Marko.** 2002. Electron tomography of frozen-hydrated isolated triad junctions. Biophys. J. **83:**2491–2501.
34. **Wartiovaara, J., L. G. Ofverstedt, J. Khoshnoodi, J. Zhang, E. Makela, S. Sandin, V. Ruotsalainen, R. H. Cheng, H. Jalanko, U. Skoglund, and K. Tryggvason.** 2004. Nephrin strands contribute to a porous slit diaphragm scaffold as revealed by electron tomography. J. Clin. Invest. **114:**1475–1483.
35. **Wu, S. R., L. Haag, L. Hammar, B. Wu, H. Garoff, L. Xing, K. Murata, and R. H. Cheng.** 2007. The dynamic envelope of a fusion class II virus: prefusion stages of Semliki forest virus revealed by electron cryomicroscopy. J. Biol. Chem. **282:**6752–6762.
36. **Zhao, H., B. Lindqvist, H. Garoff, C. H. von Bonsdorff, and P. Liljestrom.** 1994. A tyrosine-based motif in the cytoplasmic domain of the alphavirus envelope protein is essential for budding. EMBO J. **13:**4204–4211.